

A Progressive Torsion Disk-Spring Architecture for Optimization-Driven Design

Gray C. Thomas, *Member, IEEE*, Zachary Bons, *Student Member, IEEE*,
Robert D. Gregg, *Senior Member, IEEE*, Elliott Rouse, *Senior Member, IEEE*

Abstract—Progressive torsion springs have well studied applications, notably variable stiffness actuation and motion optimization. So far, nonlinear torsion spring realizations have largely relied on secondary nonlinear transmission stages to produce the appropriate torque–deflection curve from traditional linear springs. But these transmission stages introduce additional mass, volume, and complexity which has limited the practicality of the progressive spring technology. Leveraging the spring topology from in Part I, we introduce a progressive spring design that is both lighter than—and a drop-in-replacement for—a linear spring corresponding to the same peak torque and deflection. This result is achieved by virtue of efficient material utilization in cantilevered flexures. Progressive spring rates are achieved by self-collision of flexures at controlled deflections, resulting in a piecewise-linear curve. We present our design alongside an empirical validation of the design and a mathematical framework for optimizing the selection of flexures to approximate arbitrary progressive torque–deflection profiles.

I. INTRODUCTION

PROGRESSIVE torsion springs—those that become stiffer as they are deflected—offer design flexibility that can be exploited in robotic applications. Typical elastic mechanisms are defined by a single parameter, namely the stiffness coefficient of the torque–deflection relationship; however, progressive springs have additional degrees of freedom, which we term *design flexibility*, that enable a broad array of stiffening torque–deflection relationships. That is, design flexibility is the breadth of available torque–deflection curves a progressive spring architecture could achieve by adjusting the free parameters. Spring architectures with greater inherent design flexibility are advantageous to mechanism designers. Previous work has shown the benefits of progressive springs. For example, they have the potential to reduce electrical energy consumption in robotic prostheses [1]. In addition, the human ankle joint is known to operate as a progressive spring during locomotion [2]–[4], increasing the relevance of these mechanisms in bio-inspired designs [5]. Progressive springs are also key components of a popular design for variable impedance actuators [6], wherein two springs are paired as agonist and antagonist. Springs in variable impedance actuators are often quadratically progressive, which allows these mechanisms to produce a convenient linear spring rate for any pre-load [7]. However, to implement a progressive spring with

low mass, low volume, and a high degree of design flexibility is challenging.

The potential advantages of progressive springs have led to a wide variety of design implementations. One common approach is to use trigonometric changes in geometry to progressively increase the apparent stiffness. Simple configurations of pulleys [8] or bushings [9] can create a naturally progressive torsional spring-rate from linear prismatic¹ springs in tension. However, such arrangements offer little design flexibility (prompting some to add an additional linkage [10]), require many parts, and (despite co-packaging of tensioners and rotary joints [11], [12]) require large or inconvenient volumes. Thus, while they have seen use in tendon-dominated applications like articulated robot hands [13] and human-mimetic robots [14], they are less common in traditional rotary joint actuation schemes.

Another approach is to use a varying transmission ratio to emulate a progressive spring. Linkages with kinematically-varying transmission ratios can make a linear spring appear as a nonlinear spring at the mechanism output. These designs often leave several free parameters that can be chosen to shape the torque–deflection curve; for example, the literature

¹In this work, we refer to springs that deflect along a single Cartesian axis as prismatic, and springs that have a constant stiffness (either prismatic or torsional) as linear.

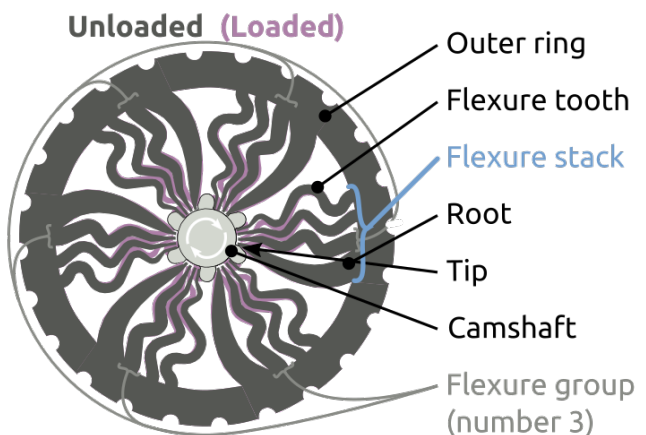


Fig. 1. Proposed spring configuration with labeled parts. Cantilevered flexure teeth extend inward from an outer ring to form the shape of a hubless wheel. These teeth can be either straight or serpentine, as depicted here, but always follow a parabolic thickness profile that guarantees near-ideal bending throughout the flexure when loaded from the tip. The tips of the teeth are designed to collide as a central camshaft is rotated, building up a stack of engaged flexures to progress the spring rate.

(G. Thomas's e-mail: gcthomas@umich.edu).

Manuscript not yet submitted Monthmonth X, 20XX; nor revised.

Color versions of one or more of the figures in this paper are available online at <https://ieeexplore.ieee.org>.

Digital Object Identifier XX.XXXX/SRO.2019.XXXXXXX

demonstrates the curve-shaping capabilities of link-lengths and similar parameters in planar four-bar linkages [15], space linkages [16], and hybrid linkage-gear drives [17]. Yet, to achieve greater design flexibility, these architectures require substantial modifications that increase mechanism complexity, mass, and volume. As an example, when designing a four bar mechanism, the torque-deflection relationship is defined by the kinematics, which significantly constrains the available torque-deflection curves available (i.e. low design flexibility). Designers that seek to increase design flexibility may choose linkages with greater degrees of freedom, however, linkages with greater degrees of freedom are less convenient and compact, among other drawbacks.

To address the design-flexibility-complexity trade-off, designers have employed cam-roller mechanisms and “wrapping cams” [18], that permit torque-deflection curves to be encoded in continuously variable geometry. Wrapping cams, like the popular compound archery bow [19], use a shaped pulley surface to achieve design flexibility by varying the effective pulley radius (and transmission ratio to the belt/cable) as a function of deflection. Wrapping cam geometries, such as a cardioid [20] or logarithmic spiral [21], can generate progressive spring rates when the belt/cable pulls a prismatic linear spring. And the geometry can be further optimized analytically, e.g. for the quadratic profile [22] (which is key in variable stiffness systems [7]), or numerically [23]. However, these designs remain limited by the volume and mass inherent in the extra transmission stage. Bidirectional springs also require a second copy of the whole system.

Unlike the voluminous wrapping cams, cam-roller systems can be quite compact, competing with wrapping cam systems even in cable-drive applications [24]. And rollers can be loaded in both directions, which allows bidirectional springs (and a stiffness adjustment if the two cams move relative to each other [13]). The approach is well suited for high-force compression springs such as die-springs or thick cantilever beams [5]. Yet, the high contact forces and required precision make these systems again a source of excess mass that, rather than integrating conveniently into other components, requires devices to be designed around their structural requirements.

Ultimately, the disadvantages of the two cam-transmission-based approaches comes down to the mass and volume disadvantages of adding a transmission. Flexure springs offer to avoid this pitfall by enabling design flexibility directly, without a secondary transmission element. However, previous designs have various limitations in mass, space, or design flexibility. Leaf springs can be progressively shortened using cams to restrict flexing, but these cams still add unnecessary mass and volume [25]. Cams placed on the tip of a flexure can control the loading against a roller, but sacrifice volume and efficient loading of the mass in the flexure itself [26]. Finally, a single-part planar torsion spring using flexure beams in a spoke-like configuration can achieve a narrow family of progressive curves efficiently in a small volume, but lacks in design flexibility, [27].

Ultimately, the field is lacking a progressive torsion spring architecture for applications where space, mass, and design flexibility are all important. The spring architecture of a gear-

like camshaft flexing a hubless wheel of inward-pointing cantilevered serpentine flexures (see Fig. 1.A) is poised to fill this gap. This architecture, as introduced in Part I, is a linear spring solution with minimal mass and a convenient disk-shaped volume that can nest inside the inner diameter of other transmission elements [28], [29]. It comes with a validated analytical model describing the spring-rate of each flexure and an automatic profile generator. This model is simple relative to FEA or even Ref. [30]’s analytical design framework for car suspension elements.

In this paper we introduce a progressive torsion spring that acts as a drop-in replacement to the springs designed in part I, retaining its advantages in mass and volume while offering a high degree of design flexibility in its progressive spring rates. Our contribution includes an empirical validation of the spring design and a mathematical framework for optimizing nonlinear torque-deflection curves to be realized with the stiffening spring design. Rather than being a heavier, bulkier, and more complex alternative, our approach results in springs that are actually lighter than the linear counterpart with equal complexity, capitalizing on the reduced energy storage of progressive springs (of equal peak torque and deflection) by efficiently using material in near-ideal bending.

II. SPRING DESIGN

Our proposed progressive torsion spring configuration (see Fig. 1) works by using a central camshaft to bend serpentine flexure teeth connected to an outer ring, similar to the linear design in Part I. And, just as in Part I, each tooth is designed according to energy storage and tip force. The key innovation is that these flexures are stacked to produce a progressive spring rate, as in a progressive quarter elliptic suspension. And our design therefore focuses on the mathematics of decomposing a torque-deflection relationship into a viable selection of tip forces, energy storage levels, and initial angle offsets. This selection would then imply the design of individual flexures that could be designed and assembled into one or more spring disks to achieve an approximation of the target torque-deflection curve.

A. A Brief Re-Introduction of the Serpentine Flexure Model

The flexure stack spring design for progressive torsion springs extends on the simple serpentine flexure model introduced in Part I. This model provides a parameterization of the flexure in terms of 1) the potential energy, \mathcal{E} , it stores at a design load, and 2) the design load at the flexure tip, F . As we shall see, the flexure stack design enables optimization over realizable progressive torque-deflection curves by leveraging the convenient structure of this parameterization. The parameterization works as follows: starting with the end-tip load, the bending moment, $\tau(x)$, on a cross-section of the flexure located at distance x from the rim is

$$\tau(x) = F(L - x). \quad (1)$$

Approximating the loading condition of this cross section as ideal bending, we can choose $\lambda(x)$ such that the two extreme edges of the cross-section are at the design stress σ_d .

$$\tau(x) = t\lambda^2(x) \quad (2)$$

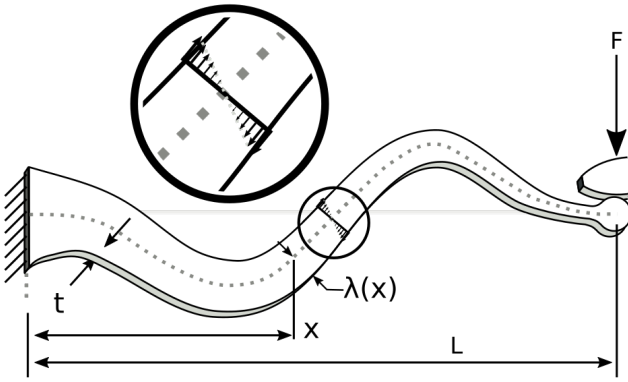


Fig. 2. Overview of the serpentine flexure loading configuration and geometric parameters. Neglecting curvature and tapering effects, the loading through cross-sections that are perpendicular to the central path can be approximated as ideal bending. Flexure width profile $\lambda(x)$ follows a square-root relationship such that entire length reaches peak bending load simultaneously, up to previously mentioned assumptions.

Each flexure tooth is a cantilever beam, and lends itself to an approximate ideal-bending analysis that neglects its shallow curvature and slow variation in thickness. Loads are applied near the flexure tip either directly from a camshaft, or indirectly by other flexure teeth.

Each flexure has a tapered thickness profile, $\lambda(x)$, that ensures an efficient use of material in ideal bending (see Fig. 2).

Due to the assumption of ideal bending, we can relate the mass, volume, and planar area of each flexure to its energy storage potential.

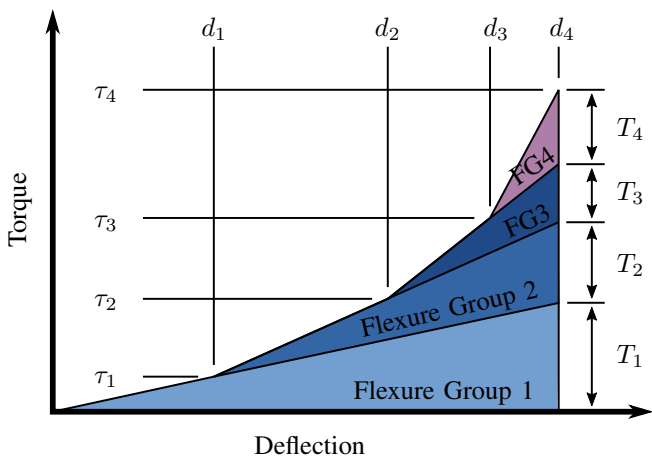


Fig. 3. Spring profile parameterization for optimization. Unknown torque variables $\tau_1, \tau_2, \dots, \tau_N$ decompose the range of torques by the number of springs. Unknown deflection variables d_1, d_2, \dots, d_N parameterize the angular offset before each flexure group engages. Each flexure group has a total torque at max deflection, T_1, T_2, \dots, T_N , as well as a total spring energy (shaded). Since flexures in a flexure group act in parallel, the area and energy are divided among the flexures in the group to determine the required spring geometry (thickness profile and serpentine factor).

B. Flexure Stacks

Mathematically, a flexure stack can be parameterized both as a list of flexures with offset angles and as a piecewise-linear torque-deflection curve. By offsetting the angle of initial engagement between different types of flexure teeth, nonlinear deflection-torque profiles can be created. Since the addition of more engaged teeth can only increase the instantaneous stiffness, nonlinear springs of this type must be stiffening. However, a naive implementation of this method of generating nonlinear flexures would require large gaps between the gear-tooth-like elements of the camshaft to accommodate angular play before the flexures are expected to engage. This disadvantage of wasted space can be avoided by designing flexures that are deflected by other flexures rather than directly by the camshaft (Fig. 5). A stack of flexures will be depressed in sequence: initially the gear-like camshaft will engage the first flexure in the series, and subsequent rotation will collide the first flexure with the second, and so on. Ultimately the process will engage the entire stack before the ultimate deflection target is reached. The local stiffness will be the sum of the stiffnesses of the currently engaged flexures, and each flexure need be designed only to allow the deflection from their initial engagement point to the target peak deflection of the entire spring.

For both the convex and non-convex optimizations, we can model the nonlinear spring as a piece-wise linear spring parameterized by N points on its torque-deflection curve (Fig. 3),

$$d(\tau) = \begin{cases} d_0 = 0 & \tau \leq \tau_0 = 0, \\ \vdots \\ d_{n-1} + \frac{d_n - d_{n-1}}{\tau_n - \tau_{n-1}}\tau & \tau_{n-1} < \tau \leq \tau_n, \\ \vdots \\ d_N & \tau > \tau_N. \end{cases} \quad (3)$$

For the convex optimization, the torque points are simply a pre-specified high-resolution decomposition of the range from zero to maximum torque. For the non-convex optimization, both the deflections and the torques will be variables.

Our mechanical spring design is only capable of rendering positive-spring rate springs that stiffen with increasing deflection, so these constraints should be enforced on the initial optimization. Fortunately, these constraints are linear in the deflections parameters, $d_i, \forall i = 0, \dots, N$.

The constraints are relatively simple. To force stiffening springs, we constrain positive and negative portions of the profile to have increasing stiffness at each junction,

$$\frac{d_{n+1} - d_n}{\tau_{n+1} - \tau_n} \leq \frac{d_n - d_{n-1}}{\tau_n - \tau_{n-1}} \quad \forall n = 0, \dots, N-1. \quad (4)$$

To force positive spring rates, we specify ascending torque points ($\tau_{i+1} > \tau_i \forall i = 1, \dots, N-1$), and then constrain deflections to similarly increase,

$$d_{i+1} \geq d_i \quad \forall i = 1, \dots, N-1. \quad (5)$$

Minimizing mass can be achieved by minimizing the stored energy in the spring at peak deflection. Applying the linear

relationship between strain energy and flexure volume in (??), the total strain energy from all the spring's flexures, U , will be linear in the total mass of all flexures, M , as

$$M = \frac{6\rho E}{\sigma_d^2} U, \quad (6)$$

where ρ is the material density, E is Young's modulus, and σ_d is the design strain. The stored energy U is the integral under the torque-deflection curve, *i.e.*

$$U = \sum_{i=0}^{N-1} (\tau_{i+1} - \tau_i) \left((d_N - d_{i+1}) + \frac{1}{2}(d_{i+1} - d_i) \right). \quad (7)$$

III. HARDWARE VALIDATION

In this section, we empirically validate our design framework by comparing three springs with differing geometries and identical desired stiffness coefficients (Fig. ??). The three springs intentionally employ different serpentine factors (see section II) to highlight the impact of the serpentine flexures. Thus, one spring (S1) was manufactured with the original straight flexures and a 33 mm radius. The second spring (S2) was manufactured with a moderate serpentine factor of 1.14, and a 33 mm radius—equivalent to that of S1. The third spring (S3) was manufactured with an aggressive serpentine factor of 1.33, but with a 28 mm spring radius—substantially smaller than that of S1 and S2 (Table I). All three springs were manufactured from SS420, and were designed with a target spring rate of 150 Nm/rad, spring thickness of 5 mm, and identical outer radius geometry to interface with the spring housing.

TABLE I

DESIGN PARAMETERS AND MEASURED PROPERTIES OF THE THREE SPRINGS. THE WEIGHT AND RADIUS OF S3 REPRESENT THE ADJUSTED VALUES FOR A THINNER OUTER RING.

Spring Design	Spring Rate (Nm/rad) Des.	Rate (Nm/rad) Exp.	Max Deflection (deg) Des.	Deflection (deg) Exp.	Serpentine Factor	Radius (mm)	Weight (g)
S1	150	155.9	14.1	14.5	1.00	33	59
S2	150	159.3	15.0	15.3	1.14	33	68
S3	150	154.9	13.2	13.5	1.33	28	52

A. Methods

B. Results

The results show accurate tracking of the nonlinear spring rate but premature yield behavior at 13 degrees. The transitions

TABLE II
SPRING RATES OF THE FOUR FLEXURE GROUPS OF THE NONLINEAR SPRING DURING LOADING AND UNLOADING. AVERAGE SPRING RATE AND PERCENT ERROR ARE ALSO SHOWN FOR EACH GROUP.

Flexure Group	Spring Rate (Nm/rad)			Error (%)	
	Desired	Actual Load	Actual Unload		
1	23.0	17.9	17.0	17.5	23.9
2	52.5	53.3	46.1	49.7	5.33
3	129.6	154.8	129.5	142.2	9.72
4	435.2	581.2	574.8	578.0	32.8

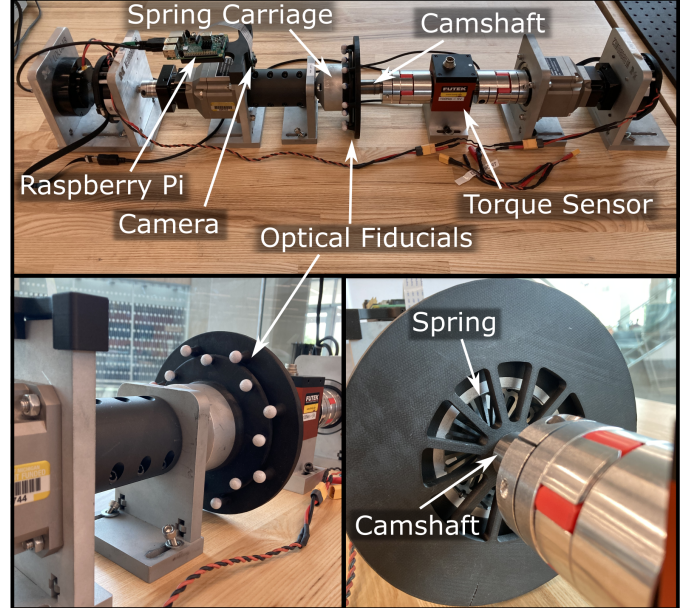


Fig. 4. Testbed used to evaluate spring performance. By tracking optical fiducials with a camera, we were able to measure true deflection of the springs.

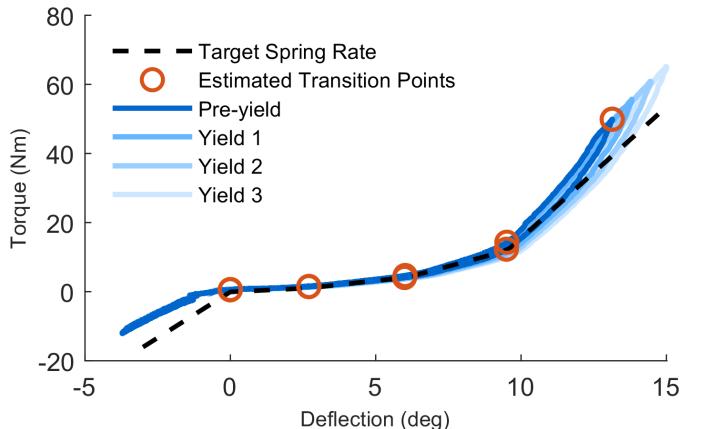


Fig. 5. Experimental profile vs designed profile.

between spring rates are observed close to the target angles (with the exception of the reverse-direction spring engagement), and the spring rates are reasonably accurate, especially for the middle two flexure groups (Tab. II). As the spring is loaded, it provides a higher torque than when it is unloaded, which is as expected for a physical spring that is not perfectly efficient. That the spring yields prematurely (*i.e.* before the target 15 degrees) can be concluded from a reduction in the torque the spring provides during loading after the first time it was cycled beyond 13 degrees. Subsequent cycles to 14, 15, and 16 degrees show the shifting level of torque the spring provides as it is slowly deformed. Since each flexure stack should have similar behavior due to symmetry of the loading condition, and since the onset angle of the final segment becomes larger with each cycle beyond the initial yield, this result shows deformation of the final flexure in each stack.

By offsetting the angle of initial engagement between different types of flexure teeth, nonlinear deflection-torque

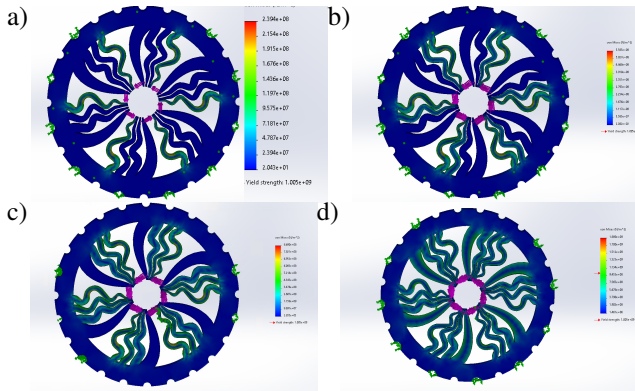


Fig. 6. Nonlinear spring FEA results at the initiation of two flexure engagement (a), three flexure engagement (b), four flexure engagement (c), and full deflection (d). Note the approximately equal stresses at the flexure boundaries in all cases.

profiles can be created. Since the addition of more engaged teeth can only increase the instantaneous stiffness, nonlinear springs of this type must be stiffening. However, a naive implementation of this method of generating nonlinear flexures would require large gaps between the gear-tooth-like elements of the camshaft to accommodate angular play before the flexures are expected to engage.

IV. NUMERICAL OPTIMIZATION

The proposed nonlinear spring design concept can render a wide range of behaviors with a huge number of parameters. And in some cases this design is amenable to traditional design. However, for large numbers of flexures, the design is more approachable via optimization. Therefore, the nonlinear spring design framework is incomplete without an analysis of how the constraints on realizable designs interact with optimizations over nonlinear torque–deflection curves.

Convexity is a key concept in optimization that describes problems where there is a unique optimum that can be found with computationally efficient solution techniques. Previous

frameworks have demonstrated that, for an appropriate parameterization of the torque–deflection curve, nonlinear springs can be optimized for several cost functions and subject to several practical constraints as a convex optimization problem [1], [31]. But, to realize a torque–deflection profile in our nonlinear spring design framework requires that each flexure has an implementable serpentine factor and flexure root thickness, and these two constraints are sadly incompatible with convex frameworks.

Therefore, to solve such optimizations for springs that can be rendered into hardware, we propose a multi-part framework. Our approach is to: first, find the ideal continuous spring profile (e.g. using high-resolution convex optimization); second, break this spring into groups that could be rendered as flexures; and third, use the grouped profile as the starting condition for a non-convex optimization that includes the constraints related to flexure geometry. Due to non-convexity, this third step will be both slow and dependent on its initial condition. Thus these first two steps are important for providing a useful first guess and a reasonable number of flexure groups (which the optimization will not be able to change). To further refine the design, the last two steps can be iterated.

Problem Definition

We consider an example optimization problem, which we frame as follows, “a good spring will be lightweight, provide a minimum SEA torque-control bandwidth (in the traditional, fixed-output sense), and ensure that noisy position measurements can be used to measure torque to an acceptable accuracy”. To create an accuracy target that is more exacting at low torques than it is at high torques, we model this torque fidelity requirement as an absolute resolution in Nm (which applies at zero torque) and a relative resolution in percentage (which applies at larger torques).

Step 1: Optimal ‘Continuous’ Spring

This problem has a trivial optimal solution: to minimize mass, the stiffest possible spring simply follows the maximum stiffness permitted by the fidelity constraint. This profile is linear up to the break torque, where the relative and absolute fidelity requirements are equivalent, and exponential after. More generally, for optimization problems without an obvious answer, convex optimization in the style of [1], [31], using a large number of points to represent the spring profile, can serve the same purpose is providing a warm start initial condition for the later optimization steps. While we call this spring continuous, it is sufficient to have very high resolution.

Step 2: Spring Splitting

To divide torque–deflection curves into groups of identical flexures, we apply a simple algorithm. In any final torque–deflection curve, each component flexure group will have a defined offset deflection d_n , peak torque T_n , and area A_n (Fig. 3). And, if we know the number of identical flexures

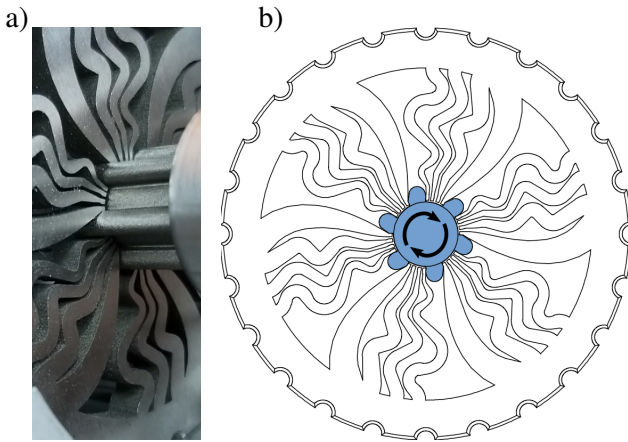


Fig. 7. Example nonlinear spring design for stiffening torque-deflection curves. As the central gear-like camshaft rotates, an increasing number of flexure teeth on the spring engage. This results in a stiffening spring rate. A) closeup of flexure-cam interface on the experimental spring; b) schematic of flexure-cam interface.

in that group, we can compute a serpentine factor: for the n^{th} flexure group comprising N_n flexures,

$$f_s = \frac{9}{2\epsilon_d^2 E \sqrt{\frac{6z(R-r)^3}{r\sigma_d}}} \sqrt{\frac{T_n}{N_n}} (d_N - d_n), \quad (8)$$

where f_s is the serpentine factor, ϵ_d is the peak design strain, E is Young's modulus, z is the plate thickness, R is the outer radius of the flexures (inner radius of the outer ring), r is the nominal contact radius of the flexure tip, and σ_d is the peak design stress.

The n^{th} flexure group comprises N_n identical flexures.

$$T_f = T_n/N_n, \quad \text{and} \quad A_f = A_n/N_n. \quad (9)$$

The serpentine factor is

SF—Stress factor (e.g. 0.9). $\sigma_d = \sigma_y \text{SF}$ —Design stress. E —Young's modulus. $\epsilon_p = \sigma_d/E$ —peak strain. $E_\epsilon = \frac{1}{2}\epsilon_p^2 E$ —Peak strain energy). $E_J = \frac{1}{2}l_f T_f$ —peak spring energy. $F_t = T_f/r$ —Tip load (r is inner radius).

$$T_n = \left(\frac{\tau_{n+1} - \tau_n}{d_{n+1} - d_n} - \frac{\tau_n - \tau_{n-1}}{d_n - d_{n-1}} \right) (d_N - d_n) \quad (10)$$

$$V_{\text{nom}} = \sqrt{6zF_t/\sigma_d} \frac{2}{3}(R-r)^{\frac{3}{2}} \quad (11)$$

$$A_{\text{nom}} = V_{\text{nom}}/z \quad (12)$$

$$E_{\text{nom}} = V_{\text{nom}} \frac{1}{3} E \quad (13)$$

$$E_{\text{nom}} = \sqrt{6zF_t/\sigma_d} \frac{2}{3}(R-r)^{\frac{3}{2}} \frac{1}{3} \frac{1}{2} \epsilon_p^2 E \quad (14)$$

$$= \sqrt{T_f} \frac{\epsilon_p^2 E}{9} \sqrt{\frac{6z(R-r)^3}{r\sigma_d}} \quad (15)$$

$$f_s = \frac{\frac{1}{2}T_f l_f}{E_{\text{nom}}} \quad (16)$$

$$f_s = \frac{9}{2\epsilon_p^2 E \sqrt{\frac{6z(R-r)^3}{r\sigma_d}}} \sqrt{T_f} l_f \quad (17)$$

$$= \frac{9}{2\epsilon_p^2 E \sqrt{\frac{6z(R-r)^3}{r\sigma_d}}} \sqrt{\frac{T_n}{N_n}} l_f \quad (18)$$

$$= \frac{9}{2\epsilon_p^2 E \sqrt{\frac{6z(R-r)^3}{r\sigma_d}}} \sqrt{\frac{T_n}{N_n}} (d_N - d_n) \quad (19)$$

To design a feasible nonlinear spring, we must ensure that for each flexure the serpentine factor, f_s , is bounded

$$1 \leq f_s \leq \bar{f}_s, \quad (20)$$

where the lower limit ensures the flexure is properly defined, and the upper limit \bar{f}_s reflects the difficulty of placing flexures with high serpentine factor near others to construct a nonlinear spring.

The lower limit on the serpentine factor must be enforced on the flexure group resulting from the optimization, but the upper limit can be ignored and dealt with by choice of the whole number of flexures in the group. If we constrain a flexure group such that

$$\frac{9\sqrt{T_n}(d_N - d_n)}{2\epsilon_p^2 E \sqrt{\frac{6z(R-r)^3}{r\sigma_d}}} \geq \sqrt{N_{\min}}, \quad (21)$$

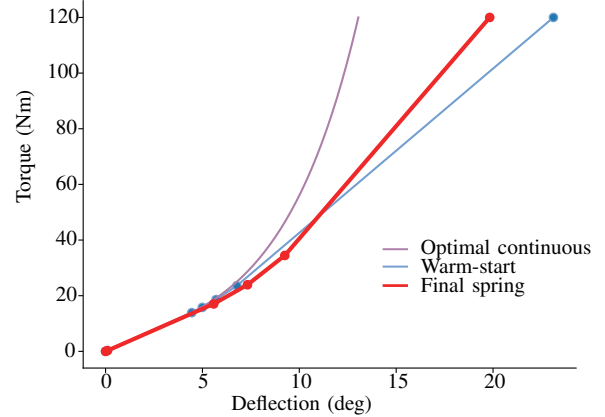


Fig. 8. The optimal torque–deflection curve generated for the example design problem. Local stiffness constraints are visualized as slope limitations on the curve. A reference linear profile is drawn to better visualize the shallow curvature.

$$\frac{9U_n}{\sqrt{T_n}\epsilon_p^2 E \sqrt{\frac{6z(R-r)^3}{r\sigma_d}}} \geq \sqrt{N_{\min}}, \quad (22)$$

then the serpentine factor we can confidently say that by choosing the highest possible number of flexures that satisfy the lower bound on s_f , we can guarantee $s_f < \sqrt{2} \approx 1.41$. If we were to instead enforce a minimum of $\sqrt{2}$ for this quantity, we could further guarantee $s_f < \sqrt{3/2} \approx 1.22$.

Step 3: Non-Convex Optimization

V. DISCUSSION

Per the hardware validation, the NL spring generally follows the desired stiffness profile, but has large errors when compared to S1–S3. In fact, the percent errors for the stiffness of flexure groups 1 and 4 exceed 20% (Tab. II). Although we have not proven anything about the source of these errors, we do have several plausible conjectures. For flexure group 1, we expected low error since there is not yet any contact between colliding flexures—the distinguishing characteristic between the linear and nonlinear stiffness designs. Thus, we postulate that the error is either caused by the difference in camshaft geometry or that this design is fundamentally unreliable for extremely soft springs. Justification for the latter point could include that the friction induced by sliding contact governs the mechanics under small loads. The larger error can be seen in flexure group 4, which led us to closely examine the design of the last (and largest) flexure. In doing so, we realized several elements of the design that are likely contributors to the poor performance. First, the flexure doesn't protrude radially from the rim of the spring. Second, the root of the flexure doesn't fully reach the prescribed radius, and third, the flexure curves in only one direction. These mistakes in the design stem from the fact that we designed and manufactured the NL spring before we had fully polished and validated the design constraints on serpentine flexures. By implementing appropriate changes and addressing these issues, it is probable

that the desired nonlinear stiffness profile could be matched with greater accuracy.

A. Broader Applicability

This spring design is robust and highly customizable, so possible applications are vast. The most significant area of impact would likely be in mobile robots that utilize SEAs, including humanoid robots, legged robots, serial-link manipulators, prosthetic limbs, exoskeletons, etc. Prostheses and exoskeletons specifically must be tunable to the needs and requirements of the user, so quick and simple replacement of differing springs could be particularly beneficial.

ACKNOWLEDGMENT

The authors would like to thank Dr. Edgar Bolívar Nieto for several fruitful discussions on the nature of convex optimization over spring profiles.

REFERENCES

- [1] E. A. Bolívar-Nieto, S. Rezazadeh, R. D. Gregg, and S. Rezazadeh, “Minimizing energy consumption and peak power of series elastic actuators: a convex optimization framework for elastic element design,” *Mechatronics*, vol. 24, pp. 1334–1345, 2019.
- [2] E. J. Rouse, L. J. Hargrove, E. J. Perreault, and T. A. Kuiken, “Estimation of human ankle impedance during the stance phase of walking,” *IEEE Transactions on Neural Systems and Rehabilitation Engineering*, vol. 22, no. 4, pp. 870–878, 2014.
- [3] A. L. Shorter and E. J. Rouse, “Ankle mechanical impedance during the stance phase of running,” *IEEE Transactions on Biomedical Engineering*, vol. 67, no. 6, pp. 1595–1603, 2019.
- [4] H. Lee, E. J. Rouse, and H. I. Krebs, “Summary of human ankle mechanical impedance during walking,” *IEEE journal of translational engineering in health and medicine*, vol. 4, pp. 1–7, 2016.
- [5] M. K. Shepherd and E. J. Rouse, “The vspa foot: A quasi-passive ankle-foot prosthesis with continuously variable stiffness,” *TRANSACTIONS ON NEURAL SYSTEMS AND REHABILITATION ENGINEERING*, vol. 25, no. 12, pp. 2375–2386, 2017.
- [6] S. Wolf, G. Grioli, O. Eiberger, W. Friedl, M. Grebenstein, H. Höppner, E. Burdet, D. G. Caldwell, R. Carloni, M. G. Catalano *et al.*, “Variable stiffness actuators: Review on design and components,” *IEEE/ASME Trans. Mechatronics*, vol. 21, no. 5, pp. 2418–2430, 2016.
- [7] C. English and D. Russell, “Mechanics and stiffness limitations of a variable stiffness actuator for use in prosthetic limbs,” *Mechanism and machine theory*, vol. 34, no. 1, pp. 7–25, 1999.
- [8] J.-i. Yamaguchi and A. Takanishi, “Development of a biped walking robot having antagonistic driven joints using nonlinear spring mechanism,” in *Proc. Int. Conf. Robotics and Automation (ICRA)*, vol. 1. IEEE, 1997, pp. 185–192.
- [9] M. Osada, N. Ito, Y. Nakanishi, and M. Inaba, “Realization of flexible motion by musculoskeletal humanoid ‘kojirō’ with add-on nonlinear spring units,” in *10th IEEE-RAS Int. Conf. Humanoid Robots*. IEEE, 2010, pp. 174–179.
- [10] O. Masahiko, I. Nobuyuki, N. Yuto, and I. Masayuki, “Stiffness readout in musculo-skeletal humanoid robot by using rotary potentiometer,” in *SENSORS, 2010 IEEE*, pp. 2329–2333.
- [11] G. Tonietti, R. Schiavi, and A. Bicchi, “Design and control of a variable stiffness actuator for safe and fast physical human/robot interaction,” in *Proc. Int. Conf. Robotics and Automation (ICRA)*. IEEE, 2005, pp. 526–531.
- [12] Z. Li, W. Chen, J. Zhang, Q. Li, J. Wang, Z. Fang, and G. Yang, “A novel cable-driven antagonistic joint designed with variable stiffness mechanisms,” *Mechanism and Machine Theory*, vol. 171, p. 104716, 2022.
- [13] M. Grebenstein, A. Albu-Schäffer, T. Bahls, M. Chalon, O. Eiberger, W. Friedl, R. Gruber, S. Haddadin, U. Hagn, R. Haslinger *et al.*, “The dlr hand arm system,” in *Proc. Int. Conf. Robotics and Automation (ICRA)*. IEEE, 2011, pp. 3175–3182.
- [14] Y. Nakanishi, T. Izawa, M. Osada, N. Ito, S. Ohta, J. Urata, and M. Inaba, “Development of musculoskeletal humanoid kenzoh with mechanical compliance changeable tendons by nonlinear spring unit,” in *Int. Conf. Robotics and Biomimetics*. IEEE, 2011, pp. 2384–2389.
- [15] R. Schiavi, G. Grioli, S. Sen, and A. Bicchi, “Vsa-ii: A novel prototype of variable stiffness actuator for safe and performing robots interacting with humans,” in *Proc. Int. Conf. Robotics and Automation (ICRA)*. IEEE, 2008, pp. 2171–2176.
- [16] M. Okada and S. Kino, “Torque transmission mechanism with nonlinear passive stiffness using mechanical singularity,” in *Proc. Int. Conf. Robotics and Automation (ICRA)*. IEEE, 2008, pp. 1735–1740.
- [17] I. Thorson and D. Caldwell, “A nonlinear series elastic actuator for highly dynamic motions,” in *IEEE/RSJ Int. Conf. on Intelligent Robots and Systems (IROS)*. IEEE, 2011, pp. 390–394.
- [18] P. H. Tidwell, N. Bandukwala, S. G. Dhande, C. F. Reinholz, and G. Webb, “Synthesis of Wrapping Cams,” *Journal of Mechanical Design*, vol. 116, no. 2, pp. 634–638, 06 1994. [Online]. Available: <https://doi.org/10.1115/1.2919425>
- [19] H. W. Allen, “Archery bow with draw force multiplying attachments,” December 1969.
- [20] B. Vanderborght, N. G. Tsagarakis, C. Semini, R. Van Ham, and D. G. Caldwell, “Maccepa 2.0: Adjustable compliant actuator with stiffening characteristic for energy efficient hopping,” in *Proc. Int. Conf. Robotics and Automation (ICRA)*. IEEE, 2009, pp. 544–549.
- [21] J. W. Hurst, J. E. Chestnutt, and A. A. Rizzi, “An actuator with physically variable stiffness for highly dynamic legged locomotion,” in *Proc. Int. Conf. Robotics and Automation (ICRA)*, vol. 4. IEEE, 2004, pp. 4662–4667.
- [22] M. Kilic, Y. Yazicioglu, and D. F. Kurtulus, “Synthesis of a torsional spring mechanism with mechanically adjustable stiffness using wrapping cams,” *Mechanism and Machine Theory*, vol. 57, pp. 27–39, 2012.
- [23] A. Schepelmann, K. A. Geberth, and H. Geyer, “Compact nonlinear springs with user defined torque-deflection profiles for series elastic actuators,” in *Proc. Int. Conf. Robotics and Automation (ICRA)*. IEEE, 2014, pp. 3411–3416.
- [24] S. A. Migliore, E. A. Brown, and S. P. DeWeerth, “Novel Nonlinear Elastic Actuators for Passively Controlling Robotic Joint Compliance,” *Journal of Mechanical Design*, vol. 129, no. 4, pp. 406–412, 04 2006. [Online]. Available: <https://doi.org/10.1115/1.2429699>
- [25] J. Malzahn, E. Barrett, and N. Tsagarakis, “A rolling flexure mechanism for progressive stiffness actuators,” in *Proc. Int. Conf. Robotics and Automation (ICRA)*. IEEE, 2019, pp. 8415–8421.
- [26] Z. Song, S. Lan, and J. S. Dai, “A new mechanical design method of compliant actuators with non-linear stiffness with predefined deflection-torque profiles,” *Mechanism and Machine Theory*, vol. 133, pp. 164–178, 2019.
- [27] É. Barrett, J. Malzahn, and N. Tsagarakis, “A compliant mechanism with progressive stiffness for robotic actuation,” in *IEEE/ASME Int. Conf. Advanced Intelligent Mechatronics (AIM)*. IEEE, 2021, pp. 774–780.
- [28] L. Mooney, K. A. Pasch, and T. D. Doan, “Planar torsion spring for knee prostheses and exoskeletons,” Aug. 24 2017, uS Patent App. 15/402,186.
- [29] A. F. Azocar, L. M. Mooney, J.-F. Duval, A. M. Simon, L. J. Hargrove, and E. J. Rouse, “Design and clinical implementation of an open-source bionic leg,” *Nature Biomedical Engineering*, vol. 4, no. 10, pp. 941–953, 2020.
- [30] S. Kim, W. Moon, and Y. Yoo, “An efficient method for calculating the nonlinear stiffness of progressive multi-leaf springs,” *Int. J. Vehicle Design*, vol. 29, no. 4.
- [31] E. A. Bolívar-Nieto, T. Summers, R. D. Gregg, and S. Rezazadeh, “A convex optimization framework for robust-feasible series elastic actuators,” *Mechatronics*, vol. 79, p. 102635, 2021. [Online]. Available: <https://www.sciencedirect.com/science/article/pii/S0957415821001112>